



Oscillatory Reaction-Diffusion Equations with Temporally Varying Parameters

S. D. WEBB*

Department of Mathematical Sciences, Loughborough University
Leicestershire, LE11 3TU, U.K.
S.D.Webb@lboro.ac.uk

J. A. SHERRATT

Centre for Theoretical Modelling in Medicine, Department of Mathematics
Heriot-Watt University, Edinburgh, EH14 4AS, U.K.

(Received and accepted March 2003)

Abstract—Periodic wave trains are the generic one-dimensional solution form for reaction-diffusion equations with a limit cycle in the kinetics. Such systems are widely used as models for oscillatory phenomena in chemistry, ecology, and cell biology. In this paper, we study the way in which periodic wave solutions of such systems are modified by periodic forcing of kinetic parameters. Such forcing will occur in many ecological applications due to seasonal variations. We study temporal forcing in detail for systems of two reaction diffusion equations close to a supercritical Hopf bifurcation in the kinetics, with equal diffusion coefficients. In this case, the kinetics can be approximated by the Hopf normal form, giving reaction-diffusion equations of λ - ω type. Numerical simulations show that a temporal variation in the kinetic parameters causes the wave train amplitude to oscillate in time, whereas in the absence of any temporal forcing, this wave train amplitude is constant. Exploiting the mathematical simplicity of the λ - ω form, we derive analytically an approximation to the amplitude of the wave train oscillations with small forcing. We show that the amplitude of these oscillations depends crucially on the period of forcing. © 2004 Elsevier Ltd. All rights reserved.

Keywords—Reaction-diffusion, Travelling waves, λ - ω systems.

1. INTRODUCTION

Periodic wave trains are the generic one-dimensional solution form for reaction-diffusion equations with a stable limit cycle in the kinetics. Such stable limit cycles are used widely in biological and chemical applications; chemical concentration waves such as those found with the Belousov-Zhabotinskii reaction are visually dramatic examples [1], other examples include the intracellular calcium system [2], and predator-prey interactions [3,4]. Periodic wave trains are solutions with constant shape and speed that oscillate in both space and time. They were first studied by Kopell and Howard [5], who showed that all oscillatory reaction-diffusion systems have a one-parameter

*Author to whom all correspondence should be addressed.

This work was supported by SHEFC Research Development Grant 107 and EPSRC (earmarked studentship to S.D.W. and advanced research fellowship to J.A.S.). S.D.W. would like to thank M. Owen (Loughborough University) for helpful discussions.

family of periodic wave train solutions; here, we use the word ‘oscillatory’ to indicate that the reaction-diffusion kinetics have a stable limit cycle.

Over the last two decades, many authors have considered the form of periodic wave trains, and their stability as solutions of the corresponding reaction-diffusion systems [6–9]. More recent work has focused on the generation of these solution forms from simple initial conditions, of the type that would arise naturally in applications [10,11]. For example, in [11], Sherratt considered the behaviour behind invasive wave fronts with initial data decaying exponentially across the domain, and showed that such initial data does indeed generate a periodic wave train. Another recent study focusing on the generation of periodic wave trains is that of Ermentrout *et al.* [10]. They consider wave train generation and interaction in equations that undergo a subcritical Hopf bifurcation and have a regime of bistability, leading to transition fronts between wave trains and homogeneous oscillations, and spatially localised oscillations.

One important difference between real ecological systems and typical reaction-diffusion models are the temporal oscillations in parameter values due to seasonal variations. Timm and Okubo [12], and Sherratt [13] studied the effects of temporal oscillations on the ability of reaction-diffusion systems to form Turing type patterns. Timm and Okubo studied a model for a predator-prey interaction between different species of plankton, with a sinusoidal temporal variation in the dispersal rate of the predator zooplankton. They presented numerical evidence that suggested that the homogeneous steady state becomes more stable as the amplitude of the temporal variation in dispersal rate increases. More recently, Sherratt [13] extended the assumptions of Timm and Okubo to include the simple case in which the temporal variation in diffusivity has a square-tooth form, alternating between two constant values. There, analytic conditions for dispersal driven patterns were determined, which show that in some cases oscillations in the predator dispersal rate can promote pattern formation.

In this paper, we consider the effects of temporal forcing on wave train propagation for systems of two reaction diffusion equations close to a supercritical Hopf bifurcation in the kinetics, with equal diffusion coefficients. In this case, the kinetics can be approximated by the Hopf normal form, giving reaction-diffusion equations of λ - ω form. λ - ω systems have been widely used in prototype studies of reaction-diffusion equations, and have proved invaluable in the study of spiral waves [14,15] and periodic plane waves [5,6]. Our objective is to understand the way in which such variations modify the generation of periodic wave trains behind invasive transition wave fronts. We do not consider the specific effects of seasonal variations in any particular ecological system; rather, we investigate the generic effect that oscillations in parameters have on oscillatory systems.

Section 2 begins by introducing reaction-diffusion systems of λ - ω type. In Section 3, we present the results of numerical simulations for λ - ω systems with temporal variation. Exploiting the mathematical simplicity of the λ - ω form, we derive analytically (Section 4) an approximation to the amplitude of the forced wave train oscillations. We then use this approximation to describe how the amplitude of these solutions depends on the period of forcing. We discuss the results in Section 5.

2. INTRODUCTION TO λ - ω SYSTEMS

We will start with an introduction to the “ λ - ω ” class of reaction-diffusion systems. These have the general form

$$\frac{\partial u}{\partial t} = \frac{\partial^2 u}{\partial x^2} + \lambda(r)u - \omega(r)v, \quad (1a)$$

$$\frac{\partial v}{\partial t} = \frac{\partial^2 v}{\partial x^2} + \omega(r)u + \lambda(r)v, \quad (1b)$$

where $r = (u^2 + v^2)^{1/2}$, and $\lambda(0)$ and $\omega(0)$ are both strictly positive. This type of equation is a standard prototype for oscillatory reaction-diffusion systems; their form facilitates analytical

study. In this paper, we will restrict attention to the case

$$\lambda(r) = \lambda_0(t) - r^2, \quad \omega(r) = \omega_0 - \omega_1 r^2, \quad (2)$$

where $\omega_0, \omega_1 > 0$, and we allow λ_0 to vary with time t . Note that, with $\lambda_0(t) = \lambda_0$ a constant, this is the normal form for kinetics close to a supercritical Hopf bifurcation, provided the variables have the same diffusion coefficient. System (1) with $\lambda_0(t) \equiv \lambda_0$, which we refer to as the ‘unforced’ case, has kinetics with a unique steady state at $u = v = 0$, which is unstable, and a stable limit cycle around that point that is circular, with radius $\lambda_0^{1/2}$.

To study these systems it is convenient to change variables from (u, v) to polar variables (r, θ) , where θ is the phase, defined by $r = (u^2 + v^2)^{1/2}$ and $\theta = \tan^{-1}(u/v)$, in terms of which (1) becomes

$$\frac{\partial r}{\partial t} = r(\lambda_0(t) - r^2) + \frac{\partial^2 r}{\partial x^2} - r \left(\frac{\partial \theta}{\partial x} \right)^2, \quad (3a)$$

$$\frac{\partial \theta}{\partial t} = (\omega_0 - \omega_1 r^2) + \frac{\partial^2 \theta}{\partial x^2} + \frac{2}{r} \frac{\partial r}{\partial x} \frac{\partial \theta}{\partial x}. \quad (3b)$$

In common with any oscillatory reaction-diffusion system, the unforced equations have a one parameter family of periodic wave train solutions [5]. The main advantage of a λ - ω system is that the form and stability of periodic plane wave solutions can be written down explicitly

$$r = R, \quad \theta = \omega(R)t \pm \lambda(R)^{1/2}x.$$

Here, the wave amplitude R parameterises the wave train family. For the unforced system given by (2) this means that periodic plane waves exist for all amplitudes $R < \lambda_0^{1/2}$. The \pm reflects the fact that the wave train can travel in either direction. Kopell and Howard [5] derived a stability condition for the periodic wave train solutions of λ - ω systems, namely that

$$4\lambda(R) \left[1 + \left(\frac{\omega'(R)}{\lambda'(R)} \right)^2 \right] + R\lambda'(R) \leq 0,$$

for linear stability. In the case of (2), this shows that the unforced periodic wave trains are stable if and only if their amplitude $R > R_c$, where $R_c = [2\lambda_0(1 + \omega_1^2)/(3 + 2\omega_1^2)]^{1/2}$.

Numerical simulations illustrating the generation of these solutions in the unforced case of (2) is shown in Figures 1a and 1b. Here, we plot the solutions for u as a function of space at successive times, with the vertical separation of successive solutions proportional to the time interval. The solutions for v have a qualitatively similar form. In these simulations, we have generated periodic waves using initial conditions consisting of an exponentially decaying perturbation to the unstable equilibrium $u = v = 0$. Specifically, we consider initial data of the form

$$u(x, 0) = v(x, 0) = A \exp(-\xi x)$$

on the semi-infinite domain $[0, \infty)$, with boundary conditions

$$\frac{\partial u}{\partial x} = \frac{\partial v}{\partial x} = 0, \quad \text{at } x = 0 \quad \text{and} \quad u, v \rightarrow 0, \quad \text{as } x \rightarrow \infty.$$

The solution evolves to a transition front moving across the domain at constant speed, and behind this front there is a periodic wave train; the direction of the wave train can be either the same or opposite to that of the front. The evolution of periodic waves from initial conditions of this form was considered previously by Sherratt [11].

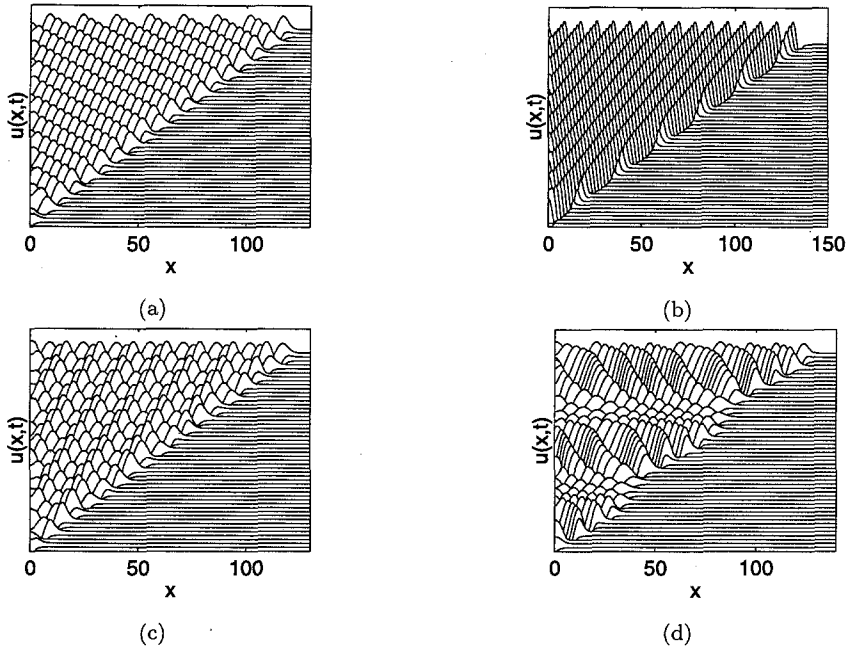


Figure 1. Typical numerical solutions of (1) showing a front moving across the domain at constant speed, with periodic wave trains behind this wave. In (a) and (b), we consider the unforced case of $\lambda(r) = \lambda_0 - r^2$ and $\omega(r) = \omega_0 - \omega_1 r^2$, where λ_0 , ω_0 , and ω_1 are constants. In (a), the wave trains move in the negative x direction, while in (b) they move in the positive x direction. In (c) and (d), we study the way in which temporal forcing modifies the periodic wave train pattern. The forcing term has the form $\lambda(r) = \lambda_0 + \epsilon f(t) - r^2$, with $f(t) = \sin(2\pi t/T)$. The temporal forcing causes spatiotemporal disturbances to the periodic wave train pattern after the invasion of a front. The figure illustrates that the amplitude of the disturbance depends crucially on the period of forcing T . We consider (1) on the semi-infinite domain $[0, \infty)$ with initial data of the form $u(x, 0) = v(x, 0) = A \exp(-\xi x)$. The parameter A affects the time course of the evolution, but has no effect on the ultimate behaviour, we take $A = 0.1$. The parameter values are: (a) $\xi = 0.8$, $\lambda_0 = 1$, $\omega_0 = 2$, $\omega_1 = 1$, $0 < t < 60$; (b) $\xi = 4$, $\lambda_0 = 3$, $\omega_0 = 1$, $\omega_1 = 1$, $0 < t < 40$. The parameter values used in (c) and (d) are $\lambda_0 = 1$, $\omega_0 = 2$, $\omega_1 = 1$, $\epsilon = 0.8$, with (c) $T = 4$; (d) $T = 23$, $0 < t < 60$. In each case, the boundary condition at $x = 0$ is zero flux, $u_x = v_x = 0$, but the solutions are essentially independent of this and the same behaviour results if one uses any fixed values for $u(0, t)$ and $v(0, t)$. In numerical solutions, the right-hand boundary is necessarily finite and we took the boundary conditions to be $u = v = 0$. The equations were solved using a Crank-Nicolson scheme. This numerical scheme, with initial data and boundary conditions, was also used in the solutions of (1) presented in the other figures.

3. TEMPORALLY VARYING PARAMETERS IN λ - ω SYSTEMS

We begin by presenting the results of numerical simulations of the λ - ω system (1) where the parameter λ_0 is allowed to vary in time. Specifically, we consider (1) with temporal forcing of the form

$$\lambda_0(t) = \hat{\lambda}_0 + \epsilon f(t), \quad f(T+t) = f(t), \quad \text{with } \frac{1}{T} \int_0^T f(s) ds = 0, \quad (4)$$

where $\hat{\lambda}_0 \gg \epsilon > 0$ and $f(t)$ has amplitude 1. Note that with $\epsilon = 0$ this reduces to the unforced case. The parameter ϵ controls the amplitude of the temporal forcing, and T is the period, and so changing the parameter T alters the period of $f(t)$ but has no effect on its amplitude. Note also that we require $f(t)$ to have mean zero.

Typical numerical solutions of (1) with (4) are shown in Figures 1c and 1d; we use a forcing function of the form $f(t) = \sin(2\pi t/T)$, but similar results are seen for a range of functional forms satisfying (4) (full details of these are given in Section 4). Initially, the solution has the same form as shown on Figure 1a, namely a wave front moving across the domain in the positive x direction. Behind this front, the temporal variation in λ_0 causes periodic disturbances to the regular wave train pattern. The amplitude and frequency of this disturbance depends upon the forcing parameters (ϵ, T) —the larger the value of ϵ , the greater the amplitude of the disturbance

to the wave train pattern. Moreover, the amplitude of the disturbance also depends on the period T of forcing, as illustrated in Figures 1c and 1d.

Further insight into the way in which the period of forcing affects the periodic wave train pattern is given by replotting the solutions such as those in Figures 1c and 1d in terms of r and $\psi = \theta_x$, rather than u and v . In the unforced case, the typical form of r is a travelling wave, moving with constant shape and speed in the positive x direction. In the region of the periodic waves, the solution amplitude r is constant. Numerical calculation of the form of the phase gradient ψ also reveals a transition wave, which changes from zero to $\psi = \pm\lambda(\hat{r})^{1/2}$, moving in parallel with the r wave. A typical form of r and ψ subject to temporal forcing of the form in (4) is illustrated in Figure 2: as a function of time t at a fixed position x (Figures 2a and 2c), and as a function of x at fixed t (Figures 2b and 2d).

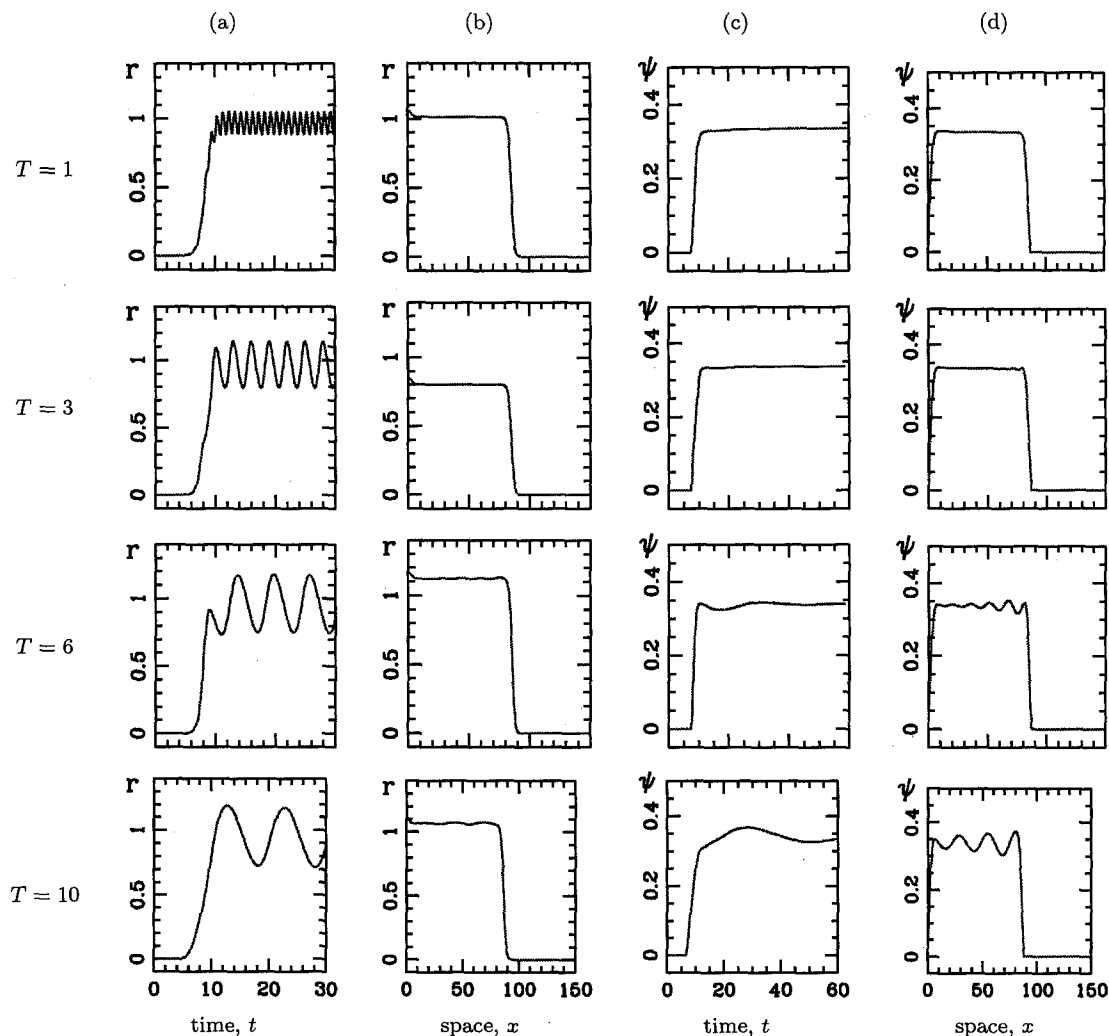


Figure 2. An illustration of the solution of (1) replotted in terms of (a),(b) r and (c),(d) $\psi = \frac{\partial \theta}{\partial x}$ in each of the four cases $T = 1, 3, 6, 10$, found via numerical solution of (1) subject to (4), with $f(t) = \sin(2\pi t/T)$. This solution shows in more detail the way in which the period of temporal forcing affects the periodic wave train patterns after invasion of a wave front. In (a) and (c), the solutions are plotted as a function of t at a fixed position x (fixed $x = 20$, $0 < x < 150$), while in (b) and (d) plotted as a function of x at fixed t (fixed $t = 45$, $0 < t < 60$). Note that in the unforced case, with $\epsilon = 0$, the temporal period of the periodic wave train is given by $T_{\text{wave}} = 2\pi/\omega(R)$, where R is the constant value of the wave amplitude r in the region of the periodic wave train. When T is small compared to T_{wave} , ψ is constant, and r demonstrates purely temporal oscillations behind the transition front. For larger values of T , these oscillations are coupled with more complicated behaviour in ψ . An interesting property of the solutions is that increasing T , with ϵ fixed, increases the amplitude of the r oscillations behind this front. The parameter values are $\lambda_0 = 1$, $\omega_0 = 2$, $\omega_1 = 1$, $\epsilon = 0.5$, giving $T_{\text{wave}} = 5.3$. The other parameters are as in Figure 1.

As in the unforced case, the solutions evolve to a transition wave moving across the domain. However, the behaviour behind the wave front consists of either regular temporal oscillations or spatiotemporal oscillations, depending on the size of T . When T is small in comparison to the temporal period of the wave train (T_{wave}), one observes regular temporal oscillations in the wave amplitude r , while as a function of space at a given time, r appears to be constant. Numerical calculation of the form of ψ reveals that ψ is constant behind this front, the same as in Figure 1a for a periodic wave train. For larger values of T , one observes more complicated behaviours in ψ , with spatiotemporal oscillations behind the wave front. Numerical simulations show that, as ϵ increases, the amplitude of the r oscillations increases. Moreover, increasing the value of T , with the amplitude of forcing ϵ fixed, also increases the amplitude of these oscillations. Figure 3 illustrates these effects on the amplitude of the oscillations in r . Intuitively, one might expect the amplitude of the r oscillations to depend on the amplitude of forcing. But, the solutions in Figure 3 suggest that the period of forcing is as important as its amplitude in determining the size of the r oscillations behind the transition wave front.

We now investigate this behaviour in more detail by constructing an analytical approximation to the solution behind the advancing wave front. We consider (1) for the simpler case in which the period of forcing T is small in comparison to T_{wave} . Note that no formal use is made of $T < T_{\text{wave}}$. Rather, we are simply interested in the form of the solution when T is small, in which ψ is constant and r demonstrates purely temporal oscillations behind the transition wave front. Our objective is to understand the way in which the amplitude of these oscillations increases with a gradual increase in the forcing period. Work in this simpler case may give us insight into the behaviour of the solutions with larger periods of forcing, in which more complicated spatiotemporal patterns are observed in the ψ solution behind the transition wave front.

4. ANALYTICAL STUDY OF SMALL PERIOD TEMPORAL FORCING

To study this behaviour analytically, we work with the equations in their polar coordinate form (3)

$$r_t = r_{xx} - r\theta_x^2 + r(\lambda_0 - r^2) + \epsilon f(t)r, \quad (5a)$$

$$\theta_t = \theta_{xx} + \frac{2r_x\theta_x}{r} + \omega_0 - \omega_1 r^2. \quad (5b)$$

We drop the hat notation on λ_0 for simplicity. If we set $\epsilon = 0$ to get the $O(1)$ system, the large time solutions of (5) must be that of the unforced system, that is $r = R$, $\theta_x = \phi$, where R is the amplitude of the unforced periodic wave train and $\phi = \pm\lambda(R)^{1/2}$, with $R^2 + \phi^2 = \lambda_0$. Since, with forcing, the full equation for r contains an ϵ term, we look for $O(\epsilon)$ corrections to r and θ_x . Substituting $r = R(1 + \epsilon\tilde{r})$ and $\theta = (\omega_0 - \omega_1 R^2)t + \phi x + \epsilon\tilde{\theta}$ into (5) and equating coefficients of ϵ gives

$$\tilde{r}_t = \tilde{r}_{xx} - \tilde{r}\phi^2 - 2\phi\tilde{\theta}_x + (\lambda_0 - 3R^2)\tilde{r} + f(t), \quad (6a)$$

$$\tilde{\theta}_t = \tilde{\theta}_{xx} + 2\tilde{r}_x\phi - 2\omega_1 R^2\tilde{r}. \quad (6b)$$

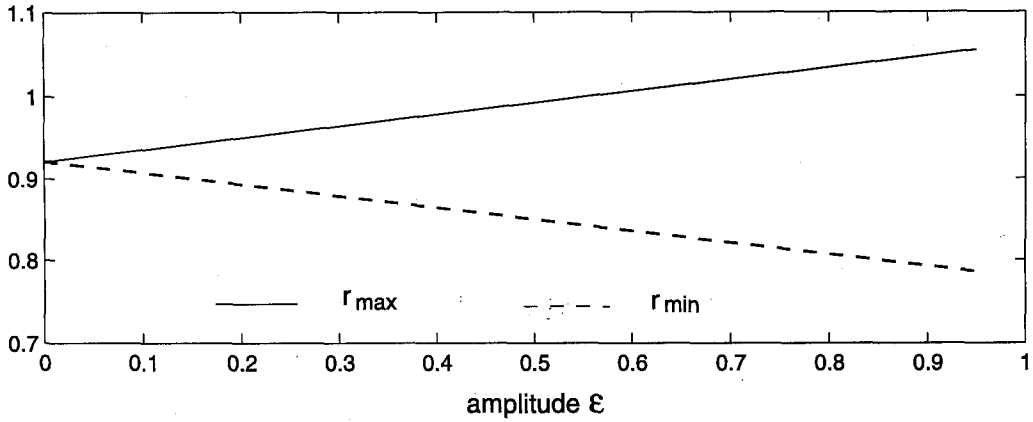
Based on the numerical observations, we look for solutions of (6) for small period forcing of the form $\tilde{r} = \tilde{r}(t)$ and $\tilde{\theta} = \tilde{\theta}(t)$. Substituting this into (6) gives

$$\tilde{r}_t = \tilde{r}(\lambda_0 - 3R^2 - \phi^2) + f(t) = -2R^2\tilde{r} + f(t), \quad (7a)$$

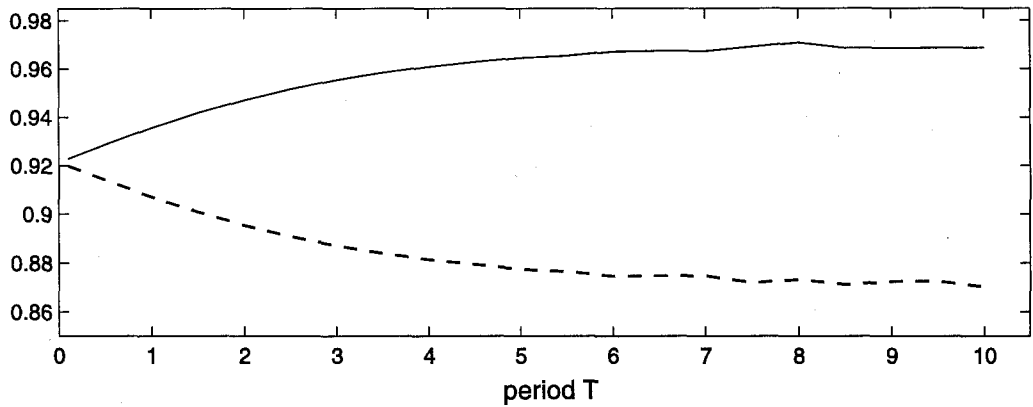
$$\tilde{\theta}_t = -2\omega_1 R^2\tilde{r}. \quad (7b)$$

Equation (7b) decouples from (7a) to order ϵ , and integrating (7a) gives

$$\frac{d}{dt} \left[e^{2R^2 t} \tilde{r} \right] = e^{2R^2 t} f(t) \Rightarrow \tilde{r}(t) = e^{-2R^2 t} \int_{\tilde{t}=0}^t f(\tilde{t}) e^{2R^2 \tilde{t}} d\tilde{t} + c_1 e^{-2R^2 t}, \quad (8)$$



(a)



(b)

Figure 3. Graphs illustrating the change in the amplitude of the r oscillations when ϵ and T are increased. Behind the wave front, r varies periodically in time. In (a), we plot the maximum and minimum values of these oscillations as a function of ϵ with the period of forcing T fixed, while in (b) plotted as a function of T with ϵ fixed. We denote these two values by r_{\max} (solid line) and r_{\min} (dotted line), respectively. The numerical values of r_{\max} and r_{\min} are given by solving (1) subject to (4) with $f(t) = \sin(2\pi t/T)$. The parameter values are $\lambda_0 = 1$, $\omega_0 = 2$, $\omega_1 = 1$, with (a) $T = 1$; (b) $\epsilon = 0.1$. The other parameters are as in Figure 1.

where c_1 is a constant of integration. In reality, we are only interested in the solution at relatively large times, and thus, we restrict attention to approximating the form of \tilde{r} as $t \rightarrow \infty$. To do this, we replace t with $nT + \tau$, where $n \in \mathbb{Z}$ and τ varies between 0 and T . We require a leading order expansion as $t \rightarrow \infty$, which implies that $n \rightarrow \infty$. Substituting $t = nT + \tau$ into (8) and replacing \tilde{t} with $t - y$ gives

$$\tilde{r}(t) = O\left(e^{-2R^2 t}\right) + \int_{\tilde{t}=0}^{nT+\tau} f(\tilde{t}) e^{2R^2(\tilde{t}-t)} d\tilde{t} = O\left(e^{-2R^2 t}\right) + \int_{y=0}^{nT+\tau} f(t-y) e^{-2R^2 y} dy.$$

This can be simplified by breaking up the interval $[0, nT + \tau]$ into the subintervals $[0, T]$, $[T, 2T]$, \dots , $[(n-1)T, nT]$ and $[nT, nT + \tau]$. Then

$$\begin{aligned} \tilde{r}(t) = O\left(e^{-2R^2 t}\right) &+ \int_{y=0}^T f(t-y) e^{-2R^2 y} dy + \int_{y=T}^{2T} f(t-y) e^{-2R^2 y} dy \\ &+ \int_{y=2T}^{3T} f(t-y) e^{-2R^2 y} dy + \dots + \int_{y=(n-1)T}^{nT} f(t-y) e^{-2R^2 y} dy. \end{aligned}$$

If we now set $\tilde{y} = y - T$ in the second integral and $\tilde{y} = y - 2T$ in the third, etc., and use the fact

that $f(nT + t) = f(t)$ for all $n \in \mathbb{Z}$, we obtain

$$\begin{aligned} \tilde{r}(t) = & O\left(e^{-2R^2t}\right) + \int_{y=0}^T f(t-y)e^{-2R^2y} dy + e^{2R^2T} \int_{\tilde{y}=0}^T f(t-\tilde{y})e^{-2R^2\tilde{y}} d\tilde{y} \\ & + e^{4R^2T} \int_{\tilde{y}=0}^T f(t-\tilde{y})e^{-2R^2\tilde{y}} d\tilde{y} + \dots + e^{2(n-1)R^2T} \int_{\tilde{y}=0}^T f(t-\tilde{y})e^{-2R^2\tilde{y}} d\tilde{y}, \end{aligned}$$

so, rearranging, we have

$$\tilde{r}(t) = O\left(e^{-2R^2t}\right) + \frac{1}{1 - e^{-2R^2T}} \int_{y=0}^T f(t-y)e^{-2R^2y} dy.$$

The leading order solution as $t \rightarrow \infty$ is then

$$\tilde{r} = \frac{1}{1 - e^{-2R^2T}} \int_{y=0}^T f(t-y)e^{-2R^2y} dy. \quad (10)$$

The term $f(\cdot)$ is a T -periodic function of time t , and thus, solution (10) is also periodic in time, with period T .

Now that we have a leading order form of \tilde{r} at large t , we consider how the amplitude of the \tilde{r} -oscillations depend on T . For the simple case of sinusoidal forcing, that is $f(t) = \sin(2\pi t/T)$, equation (10) can be integrated directly to give

$$\tilde{r} = \frac{T}{2\sqrt{\pi^2 + R^4T^2}} \sin\left(\frac{2\pi t}{T} - \beta\right), \quad (11)$$

where $\tan(\beta) = \pi/R^2T$. The amplitude of the \tilde{r} -oscillations in this case is then

$$\tilde{r}_{\text{amp}} = \frac{T}{\sqrt{\pi^2 + R^4T^2}},$$

which is an increasing function of T bounded above by $1/R^2$. A comparison between the leading order form of \tilde{r}_{amp} given by (11) and the numerical solution is illustrated in Figure 4. The comparison is very good at small values of T , but becomes worse as T is increased. This is because the solution form $\tilde{r} = \tilde{r}(t)$, $\tilde{\theta} = \tilde{\theta}(t)$ is not valid for larger periods of forcing, in which case $\phi \equiv \theta_x$ demonstrates more complicated spatiotemporal oscillations.

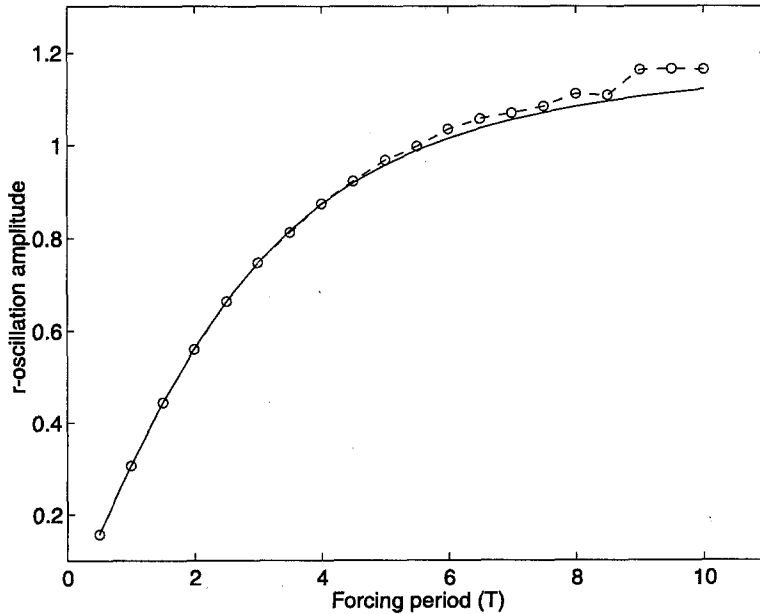


Figure 4. Graphs illustrating the comparison between approximation (11) for $f(t) = \sin(2\pi t/T)$ (solid line) with numerical solutions (o and dashed line), found via numerical solution of (1). The parameter values are $\lambda_0 = 1$, $\omega_0 = 2$, $\omega_1 = 1$, giving the unforced wave train amplitude $R = 0.914$. We take $\epsilon = 0.1$. The remaining parameters are as in Figure 1. The comparison is extremely good for small values of T , but becomes worse as T increases.

We now go on consider whether wave train solutions with general (zero-mean) forcing terms exhibit similar T dependence to the sinusoidal case. In this general case, we restrict our attention to approximating the form of \tilde{r} at its maximum and minimum values, which we denote by r_{\max} and r_{\min} , respectively. From (10)

$$\frac{d\tilde{r}}{dt} = 0 \iff \int_{y=0}^T \frac{df(t-y)}{dt} e^{-2R^2y} dy = 0. \quad (12)$$

It is convenient here to rescale (12) so that f has period 1, using $\hat{t} = t/T$ and $f(t) = g(t/T) = g(\hat{t})$. If we then replace y with $\xi = t/T - y/T$ as the integration variable, the $r_{\max/\min}$ condition (12) becomes

$$\int_{\xi=\hat{t}-1}^{\hat{t}} g'(\xi) e^{2R^2T\xi} d\xi = 0, \quad (13)$$

where prime denotes derivative with respect to ξ . The problem now boils down to finding \hat{t} in $0 \leq \hat{t} < 1$ as a function of T for which (13) is satisfied.

Typical forms for $g'(\cdot)$ and $g(\cdot)$ are sketched in Figures 5a and 5b, respectively. We restrict attention to the case of $g(\xi)$ having just two zeros in $[0, 1]$. From their definition, the functions $g'(\cdot)$ and $g(\cdot)$ are periodic with period 1 and zero mean. Without loss of generality, we consider the case where $g(\xi)$ has a maximum on $[0, 1]$ at $\xi = 0$ and a minimum at $\xi = \alpha < 1$. We also take $\xi = a$ and $\xi = b$ to be the two zeros of g , where a and b satisfy $1 > b > \alpha > a > 0$ (see Figure 5).

We begin by considering the case $\hat{t} \in [\alpha, 1]$. Figure 6 schematically illustrates the form of $g'(\xi)e^{2R^2T\xi}$ in this situation. Integral (12) is, thus, given simply by comparing the areas A_1 , A_2 , and A_3 so that $A_1 + A_3 = A_2$. Since R^2T is strictly positive, the exponential term implies that $A_1 + A_3$ increases monotonically with \hat{t} . Moreover, from Figure 6 we see that if $\hat{t} = \alpha$, then $A_3 = 0$ and $A_1 < A_2$. Similarly, if $\hat{t} = 1$, then $A_1 = 0$ and $A_3 > A_2$. Therefore, for each positive T , there is a unique $\hat{t} \in (\alpha, 1)$ satisfying $A_1 + A_3 = A_2$.

We now consider how $\hat{t} \in [\alpha, 1]$ varies with R^2T . When R^2T is small, we can approximate (13) by

$$\int_{\xi=\hat{t}-1}^{\hat{t}} \xi g'(\xi) d\xi = 0$$

and so integrating by parts gives

$$\begin{aligned} [\xi g(\xi)]_{\hat{t}-1}^{\hat{t}} - \int_{\hat{t}-1}^{\hat{t}} g'(\xi) d\xi &= 0, \\ \Rightarrow g(\hat{t}) &= 0, \\ \Rightarrow \hat{t} &= a \text{ or } b. \end{aligned} \quad (14)$$

So in $(\alpha, 1)$, we have $\hat{t} = b$ to leading order when R^2T is small. Moreover, as R^2T increases, \hat{t} decreases because the difference between A_3 and A_4 increases; eventually \hat{t} tends to α as $R^2T \rightarrow \infty$. This is illustrated in Figure 7a, with the corresponding values of $g(\hat{t})$ shown in Figure 7b. The case $\hat{t} \in [0, \alpha]$ is sketched in Figures 7c and 7d. Equation (14) implies that $\hat{t} = a$ near $R^2T = 0$ in this case. From the form of (13), such as for $\hat{t} \in [\alpha, 1]$, we see that \hat{t} becomes smaller as R^2T increases, but with \hat{t} approaching zero as $R^2T \rightarrow \infty$. Here, the solution for $g(\hat{t})$ is a monotonic increasing function of T bounded above by its maximum value.

If we now evaluate integral (12) by parts and simplify, we get

$$\int_{y=0}^T f(t-y) e^{-2R^2y} dy = \frac{f(t)}{2R^2} [1 - e^{-2R^2T}],$$

when \tilde{r} is at its maximum or minimum. Thus, substitution of this into (10) implies that a stationary value of \tilde{r} ($r_{\max/\min}$) must satisfy

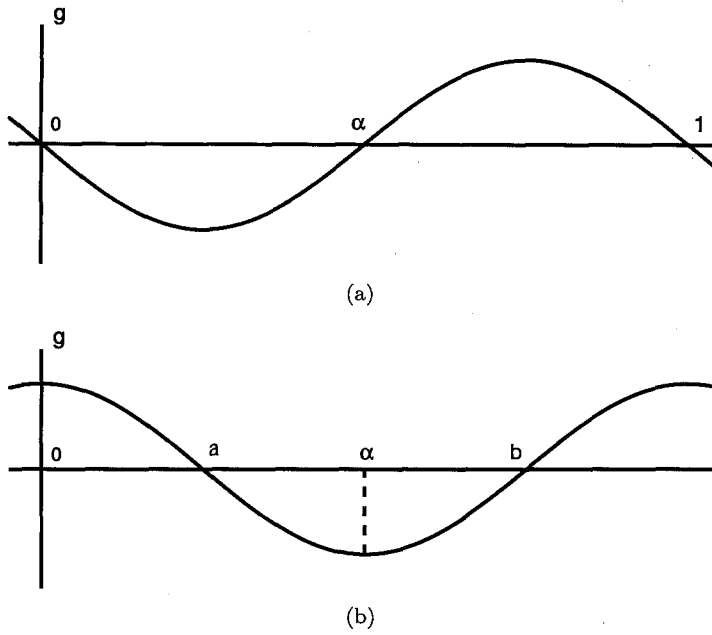


Figure 5. Schematic illustrations of the forms of (a) $g'(\cdot)$ with (b) $g(\cdot)$ satisfying (4). From their definition, the functions $g'(\cdot)$ and $g(\cdot)$ are periodic with period 1 and zero mean. We consider the case where $g(\xi)$ has a maximum on $[0, 1)$ at $\xi = 0$ and a minimum at $\xi = \alpha < 1$. We also take $g(a) = g(b) = 0$, where a and b satisfy $1 > b > \alpha > a > 0$.

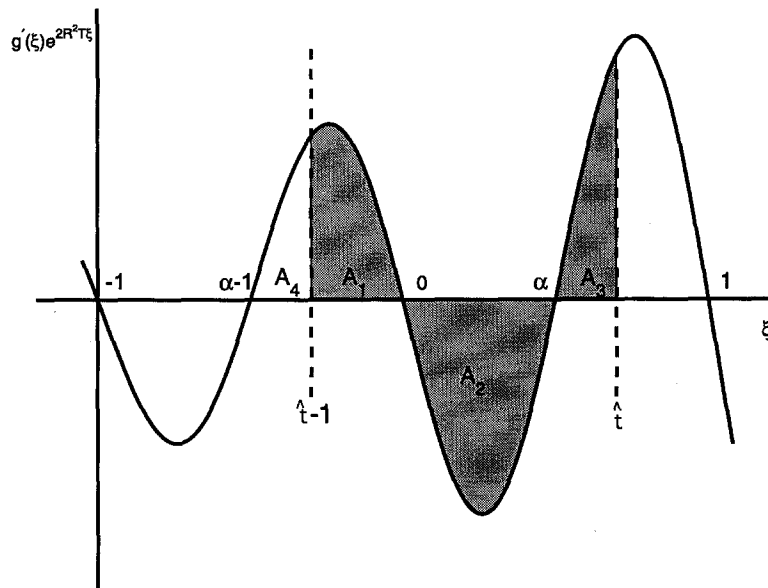


Figure 6. A schematic illustration of the form of $g'(\xi)e^{2R^2T\xi}$ plotted against ξ for a typical periodic forcing term $g(\cdot)$ given in Figure 5. Integral (12) between $\xi = \hat{t} - 1$ and $\xi = \hat{t}$ is given simply by comparing the areas A_1 , A_2 , and A_3 so that $A_1 + A_3 = A_2$. Since R^2T is strictly positive, the exponential term implies that $A_1 + A_3$ increases monotonically with \hat{t} .

$$r_{\max/\min} = \frac{f(\hat{t})}{2R^2} = \frac{g(\hat{t})}{2R^2}. \tag{15}$$

So, the form of r_{\max} and r_{\min} as functions of T are determined by $g(\hat{t})$ in Figures 7b and 7d, respectively. With these, the maximum value of \tilde{r} is, thus, a monotonic increasing function of T bounded above by $f_{\max}/2R^2$, whereas the minimum of \tilde{r} describes a decreasing monotonic form

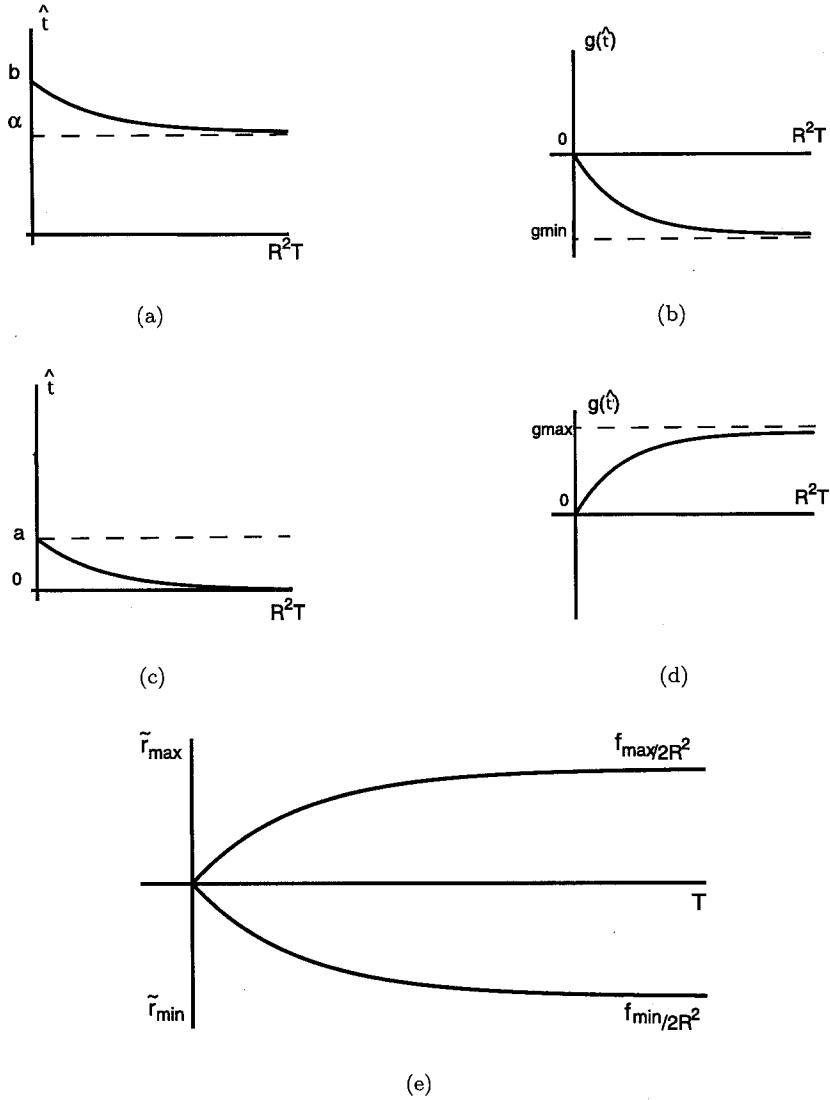


Figure 7. (a) A schematic illustration of the change in $\hat{t} \in [\alpha, 1]$ when the period of forcing R^2T is increased. Note that $\hat{t} = b$ when R^2T is small. As R^2T increases, \hat{t} decreases because the difference between A_3 and A_4 in Figure 6 increases; eventually \hat{t} tends to α as $R^2T \rightarrow \infty$. (b) The corresponding values of $g(\hat{t})$ as a function of R^2T . (c) Here, we consider $\hat{t} \in [0, \alpha]$. Note that $\hat{t} = a$ near $R^2T = 0$ in this case, with \hat{t} approaching zero as $R^2T \rightarrow \infty$. (d) $g(\hat{t})$ as a function of R^2T predicted by the form of $\hat{t} \in [0, \alpha]$ in (c). (e) The maximum and minimum values of the wave amplitude perturbation \tilde{r} given by $r_{\max/\min} = g(\hat{t})/2R^2$ with $g(\hat{t})$ in (b) and (d). The maximum value of \tilde{r} is a monotonic increasing function of T bounded above by $f_{\max}/2R^2$, whereas the minimum of \tilde{r} has a decreasing monotonic form with $\tilde{r} \rightarrow f_{\min}/2R^2$ as $T \rightarrow \infty$. Compare (e) to the examples of simple piecewise periodic forcing terms $f(t)$ defined in (16)–(18) (Figure 8).

with $\tilde{r} \rightarrow f_{\min}/2R^2$ as $T \rightarrow \infty$. This is illustrated in Figure 7e. Thus, our analysis shows that to leading order, our conclusions from the simple sinusoidal case can be extended to more general forcing terms satisfying (4). By way of example, we end this section by showing the results of a numerical investigation into three simple cases of piecewise temporal forcing, all of which satisfy (4). The three cases are as follows.

(i) Square-wave:

$$f(t) = \begin{cases} 1, & \text{if } nT \leq t < \left(n + \frac{1}{2}\right)T, \\ -1, & \text{if } \left(n + \frac{1}{2}\right)T \leq t < (n+1)T. \end{cases} \quad (16)$$

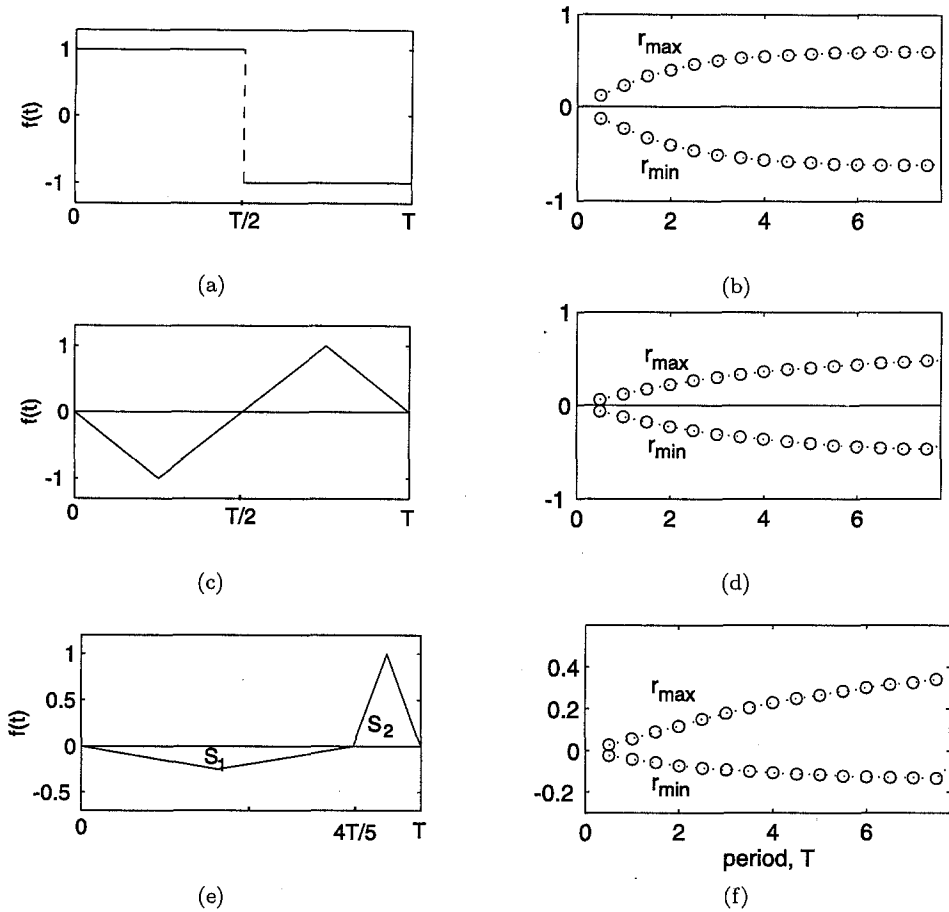


Figure 8. (a), (c), (e) Examples of simple piecewise periodic forcing terms $f(t)$ to λ_0 satisfying (4) defined in (16)–(18), respectively. Note that the areas S_1 and S_2 balance in (e) so that (4) is satisfied. (b), (d), (f) The corresponding change in the amplitude of the r -oscillations when T is increased with forcing terms given in (a), (c), and (e). We plot the the maximum and minimum values of these oscillations as a function of T with the amplitude of forcing ϵ fixed. The numerical values of r_{\max} and r_{\min} (o and dashed line) are given by solving (1) subject to (4, with (16), (17), or (18)). The parameter values in each case are $\lambda_0 = 1$, $\omega_0 = 2$, $\omega_1 = 1$, with $\epsilon = 0.1$. The other parameters are as in Figure 1.

(ii) Regular-tooth:

$$f(t) = \begin{cases} \frac{-4t}{T}, & \text{if } nT \leq t < \left(n + \frac{1}{4}\right)T, \\ \frac{4t}{T} - 2, & \text{if } \left(n + \frac{1}{4}\right)T \leq t < \left(n + \frac{3}{4}\right)T, \\ \frac{-4t}{T} + 4, & \text{if } \left(n + \frac{3}{4}\right)T \leq t < (n+1)T. \end{cases} \quad (17)$$

(iii) Skewed-tooth:

$$f(t) = \begin{cases} \frac{-5t}{8T}, & \text{if } nT \leq t < \left(n + \frac{2}{5}\right)T, \\ \frac{5t}{8T} - \frac{1}{2}, & \text{if } \left(n + \frac{2}{5}\right)T \leq t < \left(n + \frac{4}{5}\right)T, \\ \frac{10t}{T} - 8, & \text{if } \left(n + \frac{4}{5}\right)T \leq t < \left(n + \frac{9}{10}\right)T, \\ \frac{-10t}{T} + 10, & \text{if } \left(n + \frac{9}{10}\right)T \leq t < (n+1)T, \end{cases} \quad (18)$$

where $n \in \mathbb{Z}$ in all cases.

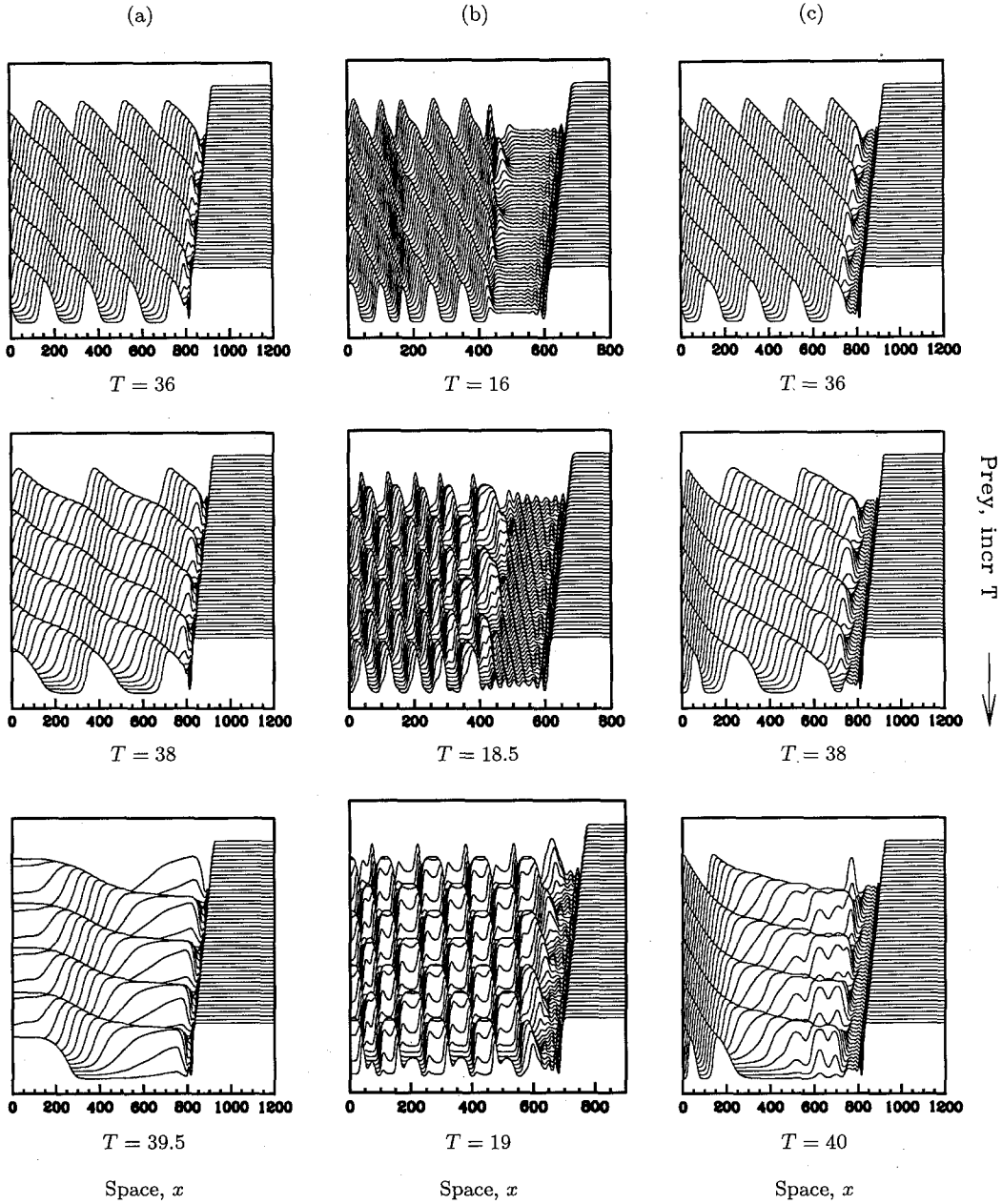


Figure 9. An illustration of invasion of a prey population by predators with temporally varying parameters. The solutions shown are for a standard predator-prey model of the form $\frac{\partial h}{\partial t} = D_h \frac{\partial^2 h}{\partial x^2} + f_h(h, p, t)$, $\frac{\partial p}{\partial t} = D_p \frac{\partial^2 p}{\partial x^2} + f_p(h, p, t)$, with oscillatory kinetics; here h and p denote the prey and predator densities, respectively. We plot the prey density h as a function of space at successive times. The solution of the predator density p has a qualitatively similar form. Initially, the system is in the prey-only steady state everywhere except near the $x = 0$ boundary where predators are introduced. This initial perturbation spreads through the domain corresponding to the invasion of the prey population by predators. Immediately behind the invading wave front, the solutions are close to the (unstable) coexistence steady state, and further back periodic travelling waves develop. The kinetic functions used are $f_p(h, p) = p(ach/(1+ch) - 1)/ab$, $f_h(h, p) = h(1-h) - cph/(1+ch)$. We show the effects of varying each of the kinetic parameters independently with sinusoidal forcing. The parameters used are (a) $a(t) = 3 + 0.085 \sin(2\pi t/T)$, $b = 4$, $c = 3$ with $T = 36, 38, 39.5$; (b) $b(t) = 4 + 0.7 \sin(2\pi t/T)$, $a = 3$, $c = 3$ with $T = 16, 18.5, 19$; (c) $c(t) = 3 + (3.2 \times 10^{-4}) \sin(2\pi t/T)$, $a = 3$, $b = 4$ with $T = 36, 38, 40$. In graph (b), the temporal variation induces a disturbance to the wave train pattern which depends on the forcing period in a very similar manner to that in $\lambda - \omega$ systems. In graphs (a) and (c), changing T alters the average speed of the travelling wave train behind the advancing front in addition to its amplitude. In each case, the boundary condition at $x = 0$ is zero flux $h_x = p_x = 0$, plotted for (a),(b) $900 < t < 1000$ and (c) $1800 < t < 2000$. The equations were solved numerically using a Crank-Nicolson scheme.

Solving (1) with (16), (17), or (18) gives solutions of the same basic form, as illustrated in Figure 2, namely an advancing front of the wave train amplitude moving across the domain, with either regular temporal or spatiotemporal oscillations behind it. We have found that the amplitude of such oscillations increase with T , in a manner very similar to that for the sinusoidal forcing. In particular, these solutions reproduce exactly the same qualitative behaviour that we predict in Figure 7 for general forcing terms. The form of $f(\cdot)$ with numerically calculated values for \tilde{r}_{\max} and \tilde{r}_{\min} in each case (16)–(18) is illustrated in Figure 8.

5. DISCUSSION

Periodic wave trains are the generic solution form for reaction-diffusion equations in one space dimension in which the kinetics have a limit cycle. Many systems in biology and chemistry are oscillatory, with classic examples including the Belousov-Zhabotinskii reaction [1], and the intracellular calcium system [2]. In ecology, spatiotemporal field data on cyclic populations is generally too limited for the detection of periodic plane waves. However, recent data on vole populations in the Kielder forest (Northern U.K.) has presented evidence for the presence of such waves [16,17]. Here, the authors use statistical techniques to show that the observed spatially asynchronous, oscillating vole populations correspond to a periodic wave train. Cyclic populations such as the field vole are subject to strong temporal forcing by seasonal variations, and this represents one of the main points of difference between real ecological systems and the theoretical models used to study them. In this paper, we have considered the effect of temporal variations on the behaviour of solutions to oscillatory reaction-diffusion equations. Rather than study the ecological details of a particular case, our focus has been on the generic effects on periodic forcing in kinetic parameters.

We have investigated temporal forcing in systems of two reaction diffusion equations close to a supercritical Hopf bifurcation in the kinetics, with equal diffusion coefficients. In this case, the kinetics can be approximated by the Hopf normal form, giving equations of λ - ω type. Numerical solutions of this model show that temporal variation leads to oscillations of the wave train amplitude, which is constant in the unforced situation. An interesting result is that the amplitude of these oscillations becomes larger as the period of temporal forcing increases. Plotting these solutions in terms of the wave train amplitude and phase gradient reveals details of this forcing, and we used this to derive an approximation to the amplitude of the forced wave train solutions for small period temporal forcing, valid to leading order at large times. We then use this approximation to describe in detail how these solutions depend on the period of forcing for general periodic forcing terms with zero mean.

Some of the open questions related to this problem concern the form, and in particular the speed of the advancing front of wave amplitude, via which periodic waves are generated in our numerical simulations. Work is in progress on investigating the transition front, but we briefly summarize some of our recent findings here (full details of this will be presented elsewhere). In the unforced case, the wave amplitude evolves to a transition front moving with constant shape and speed. In this paper, we have shown that temporal forcing causes the wave amplitude to oscillate behind this front. In addition to this, we have observed in subsequent simulations that the speed of the advancing front in the temporally forced case is also periodic (data not shown). So far, we have investigated this by linearising the r - θ equations, and using simple intuitive criteria, to derive an analytic expression for both the oscillating speed and form of this advancing front. These analytical predictions compare very well with numerical solutions of the λ - ω PDEs at the leading edge of the advancing front, but do not compare so well for solutions towards the tail of the transition front. This is because, although the different points on the transition wave front oscillate with the same average speed, we have found that the amplitude of these oscillations actually increases towards the tail of the transition front. Understanding this behaviour is an important challenge for our future research.

Many authors have used λ - ω systems as a prototype for reaction-diffusion equations whose kinetics have a limit cycle. It is, therefore, natural to ask whether similar behaviour is observed in more general oscillatory reaction-diffusion systems. In models of this type, the classic solution is a wave of invasion of one equilibrium state by another. For example, a wave of pursuit by a predator species and of evasion by its prey; ahead of the wave there are prey but no predators, and behind the wave the two species coexist. Here, the rear of the invasive wave front will impose an exponentially decaying perturbation to the unstable coexistence equilibrium, which will in turn give rise to periodic plane waves [18]. This is not possible in any system of λ - ω type, as there is no equivalent of the prey-only steady state.

We have investigated temporal varying parameters numerically in a set of standard predator-prey kinetics, all of which have a stable limit cycle for appropriate parameter values, and we did indeed find very similar behaviour (see Figure 9). However, these solutions also demonstrated behaviour which was not observed in the λ - ω case. In the predator-prey model, changing T also affected the average speed of the wave train behind the advancing front, as well as its amplitude. This new behaviour is not unexpected, however, since varying the kinetic parameters in the more general reaction-diffusion system corresponds to varying parameters λ_0 , ω_0 , and ω_1 simultaneously, whereas the work described in this paper applies only to the case in which λ_0 varies in time. The fact that the ω_0 and ω_1 parameters affect the phase of the solutions, whereas λ_0 affects its amplitude, suggests that ω_0 and ω_1 variations may give new behaviour not seen with simple λ_0 forcing.

The temporal forcing of the various other λ - ω parameters in the problem is an obvious extension to this work, and would give a fuller picture of the response of oscillatory reaction-diffusion systems to temporal variations. Nevertheless, the analysis with λ_0 -forcing has given considerable insight into effects of temporal variations; in particular, the way in which the period of the temporal forcing can modify the amplitude of the wave train patterns behind invasion.

REFERENCES

1. J.A. Leach, J.H. Merkin and S.K. Scott, Oscillations and waves in the Belousov-Zhabotinskii reaction in a finite medium, *J. Math. Chem.* **16**, 115–124, (1994).
2. J. Sneyd, J. Keizer and M.J. Sanderson, Mechanisms of calcium oscillations and waves: A quantitative analysis, *FASEB J.* **14**, 1463–1472, (1995).
3. M.P. Hassell, H.N. Comins and R.M. May, Spatial structure and chaos in insect population dynamics, *Nature* **353**, 255–258, (1991).
4. R.M. May, *Stability and Complexity in Model Ecosystems*, Princeton Univ. Press, (1981).
5. N. Koppell and L.N. Howard, Plane wave solutions to reaction-diffusion equations, *Stud. Appl. Math.* **52**, 291–328, (1973).
6. G.B. Ermentrout, Small amplitude stable wave trains in reaction-diffusion systems, *Lect. Notes Pure Appl. Math.* **54**, 217–228, (1980).
7. S. Koga, Coexistence of stably propagating periodic wave trains in intrinsically bistable reaction-diffusion systems, *Phys. Lett. A* **191**, 251–256, (1994).
8. K. Maginu, Stability of periodic travelling wave solutions with large spatial periods in reaction-diffusion systems, *J. Diff. Eqns.* **39**, 73–99, (1981).
9. H.G. Othmer, Current problems in pattern formation, *Lect. Math. Life Sci.* **9**, 57–86, (1977).
10. G.B. Ermentrout, X. Chen and Z. Chen, Transition fronts and localized structures in bistable reaction-diffusion equations, *Physica D* **108**, 147–167, (1997).
11. J.A. Sherratt, On the evolution of periodic plane waves in reaction-diffusion systems of λ - ω type, *SIAM J. Appl. Math.* **54**, 1374–1385, (1994).
12. U. Timm and A. Okubo, Diffusion-driven instability in a predator-prey system with time-varying diffusivities, *J. Math. Biol.* **31**, 307–320, (1992).
13. J.A. Sherratt, Turing bifurcations with temporally varying diffusion coefficient, *J. Math. Biol.* **33**, 295–308, (1995).
14. J.M. Greenburg, Spiral waves for λ - ω systems, *Adv. Appl. Math.* **2**, 450–455, (1981).
15. S. Koga, A variety of stable persistent waves in intrinsically bistable reaction-diffusion systems—From one-dimensional periodic waves to one-armed and 2-armed rotating spiral waves, *Physica D* **84**, 148–161, (1995).
16. X. Lambin, D.A. Elston, S.J. Petty and J.L. Mackinnon, Spatial asynchrony and periodic travelling waves in cyclic populations of field voles, *Proc. R. Soc. Lond. B* **265**, 1491–1496, (1998).

17. J.L. MacKinnon, S.J. Petty, D.A. Elston, C.J. Thomas, T.N. Sherratt and X. Lambin, Scale invariant spatio-temporal patterns of field vole density, *J. Anim. Ecol.* **70**, 101–111, (2001).
18. J.A. Sherratt, B.T. Eagan and M.A. Lewis, Oscillations and chaos behind predator-prey invasion: Mathematical artifact or ecological reality?, *Phil. Trans. R. Soc. B* **352**, 21–38, (1997).